Defective Lattice Charge Density Waves in $La_{10}Se_{19}$, Cs_3Te_{22}, $RbDy_3Se_8$, and $Dy_{65.33}Se_{120}$

Stephen Lee* and Brendan J. Foran

Contribution from the Department of Chemistry, University of Michigan, Ann Arbor, Michigan 48109-1055

Received June 16, 1995. Revised Manuscript Received July 10, 1996[⊗]

Abstract: In this paper we consider charge density waves in defective lattice structures. Just as in nondefective lattices, we find that the Fermi surface plays an important role in supercell dimensions. In particular, a correspondence is found between the Fermi surfaces of the defective and the nondefective lattices. The concept of an effective band filling is introduced, which may be understood as the band filling for which the fully occupied lattice mimics the Fermi surface of the partially occupied lattice. To demonstrate the efficacy of this method, the superstructures of $La_{10}Se_{19}$, Cs_3Te_{22}, $RbDy_3Se_8$, and $Dy_{65.33}Se_{120}$ are studied. Fermi surfaces from both Hückel and extended Hückel tight-binding theories allow the rationalization of the defect lattice structures found in these systems. Finally a simple model based only on nearest neighbor interaction is found to preserve most of the essential features of the Hückel and extended Hückel treatments.

Introduction

In the last few years, tight-binding methods have been applied with remarkable efficacy to the rationalization and prediction of both commensurate and incommensurate charge density waves (CDW's).[1,2] These CDW's modulate the sublattice atom positions away from their ideal sublattice sites.[3,4] The tight-binding studies used to account for such CDW's are in general based on a calculation of the sublattice Fermi surface, followed by the determination of those reciprocal space or *k*-vectors[5,6] which allow maximum interaction between opposing states on the Fermi surface.

While authors have applied this method of nested *k*-vectors to the problem of CDW's, there has been little treatment of the parallel problem of defective lattice CDW's (d-CDW's).[7] A d-CDW is one in which crystalline superstructures are produced by an ordered pattern of vacancies over the original sublattice in addition to any coexisting CDW's. In this paper we show how the method of nesting vectors can be applied to the defect lattice CDW problem. We apply this method to both the one-dimensional chain and the two-dimensional square lattice. These latter results are directly applied to the square lattice d-CDW's found in $La_{10}Se_{19}$,[8] Cs_3Te_{22},[9] $RbDy_3Se_8$,[10] and $Dy_{65.33}Se_{120}$.[11]

Effect of Site Defects on Band Structure

Both the extended Hückel[12,13] (eH) and Hückel methods have been applied to CDW's in systems without site defects. In these calculations one considers a tight-binding Hamiltonian for which the off-diagonal form is given by the Wolfsberg−Helmholz approximation:[14]

$$H_{ij} = \frac{K}{2} S_{ij}(H_{ii} + H_{jj}) \tag{1}$$

where i and j are atomic orbital indices, H_{ii} and H_{jj} are predetermined Coulombic integrals, S_{ij} is the overlap integral between i and j, and K is a constant generally set at the value 1.75. In the case of Hückel theory one solves the equation $H\psi = E\psi$ while for the eH method one solves $H\psi = ES\psi$. One generally considers all interatomic interactions between atoms less than 10 Å apart.

For systems with translational symmetry, the solutions of the Hückel or eH equations are Bloch functions of the form

$$|\psi(\vec{k})\rangle = \sum e^{2\pi i \vec{k}\cdot\vec{r}_i} c_i |\phi(\vec{r}_i)\rangle \tag{2}$$

where $\phi(\vec{r}_i)$ is an atomic orbital located at the position $\vec{r}_i$ in real space, and $\vec{k}$ is the crystal momentum vector. The vector $\vec{k}$ is in the same units as those used by crystallographers when describing reciprocal space.[15]

The use of such $\vec{k}$-vectors allows one to reduce the infinite dimensional crystalline problem to one of dimension N, where N represents the number of atomic orbitals located inside the crystallographic unit cell. For example, in the case of a zigzag chain of s orbitals, **1**,

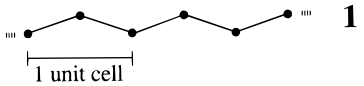

1

there are two orbitals per unit cell and the corresponding

* Author to whom correspondence should be addressed.

[⊗] Abstract published in *Advance ACS Abstracts,* September 1, 1996.

(1) Whangbo, M.; Canadell, E.; Foury, P.; Pouget, J. *Science* **1991**, *252*, 96.
(2) Canadell, E.; Whangbo, M. *Chem. Rev.* **1991**, *91*, 965.
(3) Wilson, J. A.; DiSalvo, F. J.; Mahajan, S. *Adv. Phys.* **1975**, *24*, 117.
(4) Monceau, P.; Ong, N. P.; Portis, A. M.; Meerschaut, A.; Rouxel, J. *Phys. Rev. Lett.* **1976**, *10*, 602.
(5) Burdett, J. K. *Chemical Bonding in Solids*; Oxford University Press: New York, 1995.
(6) Hoffmann, R. *Solids and Surfaces: A Chemist's View on Bonding in Extended Structures*; VCH Publishers, Inc.: New York, 1988.
(7) Jellinek, F. In *Inorganic Sulphur Chemistry*; Nickless, G., Ed.; Elsevier Publishing Company: Amsterdam, 1968; pp 680 and 702.
(8) Grupe, M.; Urland, W. *J. Less.-Common Met.* **1991**, *170*, 271.
(9) Sheldrick, W. S.; Wachhold, M. *Angew. Chem., Int. Ed. Engl.* **1995**, *34*, 450.
(10) Foran, B.; Lee, S.; Aronson, M. *Chem. Mater.* **1993**, *5*, 974.
(11) van der Lee, A.; Hoistad, L.; Evain, M.; Foran, B.; Lee, S. *Chem. Mater.* Submitted for publication.
(12) Hoffmann, R. *J. Chem. Phys.* **1963**, *39*, 1397.
(13) Whangbo, M.; Hoffmann, R.; Woodward, R. B. *Proc. R. Soc.* **1979**, *A366*, 23.
(14) Wolfsberg, M.; Helmholz, L. *J. Chem. Phys.* **1957**, *20*, 83.

S0002-7863(95)01965-2 CCC: $12.00

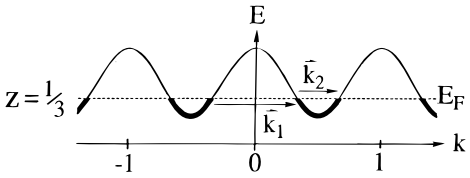

Figure 1. Energy of an infinite chain of p_x orbitals as a function of reciprocal space index, k. Thick portions of the sinusoidal curves represent filled bonding orbitals.

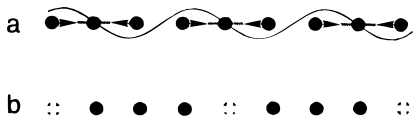

Figure 2. (a) CDW for the one-dimensional chain where $k_2 = {}^1/_3$. Arrows indicate shifts in atomic positions going from the 1-atom subcell to the 3-atom supercell. (b) d-CDW where $q = {}^3/_4$. Note the equivalent formation of trimers in parts a and b.

Hamiltonian is

$$H(\vec{k}) = \begin{pmatrix} \alpha & \beta(1 + e^{2\pi ik}) \\ \beta(1 + e^{-2\pi ik}) & \alpha \end{pmatrix} \qquad (3)$$

where α and β are the standard Hückel α and β terms, and where we have chosen one unit cell to be of length 1.

1-D d-CDW

Our discussion of d-CDW systems will be facilitated by first reviewing the nondefective CDW model. Here we consider an infinite linear chain of p_x orbitals running in the x direction. Consider the one atom primitive unit cell and nearest neighbor interactions only. The band structure of this system is shown in Figure 1. In Figure 1, we also include a band filling, z ($0 \leq z \leq 1$), where $z = 0$ and 1 denote respectively the empty and fully occupied bands. Filled orbitals are represented by the thick line portion of the sinusoidal curve, while empty crystal orbitals are represented by thin lines. The intersection between these thick and thin lines represents the 1-D Fermi surface. Two vectors connect points on the Fermi surface. In Figure 1 they are shown as k_1 and k_2. It may be seen that $k_1 + k_2 = 1$ and that k_2 corresponds to z, the fractional band filling.

In order for the HOMO and LUMO (highest occupied and lowest unoccupied orbitals) to mix, a lowering of symmetry must occur which causes either k_1 or k_2 to become a new reciprocal crystal lattice vector. For example, in the case where $z = {}^1/_3$, then $k_2 = {}^1/_3$. As the original reciprocal lattice corresponds to integer values along the k axis shown in Figure 1, the new k_2 vector therefore causes a tripling of the number of permissible diffraction reflections and thus a tripling of the unit cell length. This k_2 vector is the crystal momentum vector of a wave of the form $\cos(2\pi k_2 r + \theta)$ where r represents the coordinates with the unit length and θ is an arbitrary phase angle. It is instructive to look at the amplitude of this wave at true atomic sites. For illustrative purposes we choose $\theta = \pi/2$. As is shown in Figure 2a, one of three atom sites in the new unit cell lies at a node while the remaining two atoms lie in zones of alternately positive and negative wave amplitudes. If we now consider these values as shifts in the position of the atoms along the x direction, Δx (positive amplitudes $= +\Delta x$; negative amplitudes $= -\Delta x$), then as is shown in Figure 2a, this wave corresponds to the formation of somewhat isolated trimers along the chain. As there are three orbitals per trimer and the band filling was assumed to be ${}^1/_3$, there is therefore a gap which has opened up at the Fermi surface. There is a second parallel solution for the choice of the nesting vector, k_1. Often in one dimension, the k vector which is shortest corresponds most naturally to the lowest energy distortion. For the case of $z = {}^1/_3$, the k_2 vector is ${}^1/_3$, while $k_1 = {}^2/_3$. Above the half-filled band, however, k_1 is shorter than k_2. One useful way of viewing the change from k_2 to k_1 as the key branch of the Fermi surface is to recall that in alternate systems like the 1-D (or square lattice), for each and every bonding orbital with net bonding energy E, there is an antibonding orbital with an equal and opposite antibonding energy, $-E$. One consequence of this symmetry is that a system with N electrons has exactly the same Fermi surface shape as one with N holes. Let us define t as the fraction of holes in the system with $t \equiv 1 - z$. We find for example the system for which $t = {}^2/_5$ has the same Fermi surface as the system where $z = {}^2/_5$. For $z \leq {}^1/_2$, it is most convenient to view the CDW's or d-CDW's in the electron picture while for $z \geq {}^1/_2$, the hole picture is more convenient.

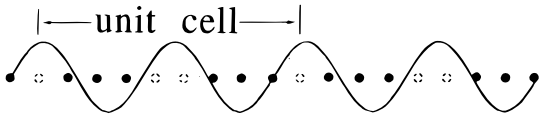

Figure 3. One unit cell of the one-dimensional defect latice pattern for $z = {}^2/_3$ and $q = {}^2/_3$. Defect sites represented by dotted circles are placed at sites with maximal wave amplitude.

We now consider as a first example of a d-CDW a defect lattice of this same linear chain in which every fourth atom has been removed. This pattern is illustrated in Figure 2b. As can be seen in the figure, this defect pattern leads to the formation of relatively isolated trimers and hence will cause band gaps at fractional band fillings of ${}^1/_3$ and ${}^2/_3$. The overall effect of this defect pattern is to create the band gaps at the same band fillings as those found in the nondefect (displacive) CDW shown in Figure 2a.

This example leads to a natural question of whether it is possible in general to find a connection between the well-understood displacive CDW's and the less well-characterized defect CDW's. As we will show below rigorous analogies between the two types of CDW's exist. We consider first the linear chain of p_x orbitals and as the chemical systems studied in this paper are electron rich, we consider systems where $z \geq {}^1/_2$ or equivalently $t \leq {}^1/_2$.

Theorem: Consider a defective linear chain of p_x orbitals running in the x-direction with nearest neighbor interactions only and with lattice sites placed at unit distances apart. Let the fractional site occupation (i.e., the fraction of all lattice sites which are filled) be q and the fractional hole filling be t where $t \leq {}^1/_2$. Consider the CDW for the nondefective lattice, $\cos(2\pi k'_1 r + \theta)$ where $k'_1 \equiv t' \equiv qt$. Place defect sites at the maximal values of this function, choosing θ in such a way so that this assignment is unambiguous. Then the resulting defect structure has a band gap at the hole filling of t (i.e., at a band-filling of $z = 1 - t$).

Before proving this theorem, we give an illustrative example of its use. As an example, consider the case $q = {}^2/_3$ and $z = {}^2/_3$. As $z > {}^1/_2$, we use the hole formalism. We find $t = 1 - {}^2/_3 = {}^1/_3$ and that $t' = ({}^1/_3)({}^2/_3) = {}^2/_9$. In Figure 3 we plot the function $\cos(2\pi r({}^2/_9) + \pi/2)$. We further place the actual defects at those values where this wave has its greatest amplitude. As there are three defects per nine sites, we choose the three sites with greatest wave amplitude. Figure 3 shows the resultant structure consists of two trimers separated by alternately one and two neighboring defect sites. As $z = {}^2/_3$, the four resulting bonding or nonbonding orbitals are filled while the remaining two antibonding orbitals remain empty. There is therefore a

(15) Stout, G. H.; Jensen, L. H. *X-ray Structure Determination. A Practical Guide*, 2nd ed.; John Wiley & Sons: New York, 1989.

band gap at the Fermi energy. Similar patterns are found for other choices of the phase angle, θ. We now prove the general result.

Proof: Let the fractional site occupancy $q = N/M$ and the fractional hole band filling $t = K/L$ where N and M as well as K and L are relatively prime integers. By assumption $t' = NK/ML$. We may therefore consider a unit cell of length ML. In this unit cell the wave $\cos(2\pi t'r + \theta)$ has NK maxima. Assume for now there are enough defects to place one near every maximum. Therefore each unit cell has been divided into NK fragments of near equal length. There are a total of $q \cdot ML$ atoms in the unit cell. As $q = N/M$, the total number of atoms equals NL. The average length of each segment is the total number of atoms divided by the total number of fragments. The average length of each segment is $NL/NK = L/K$. Now let $L = jK + i$ where $i < K$. We therefore can have Ni segments of length $j + 1$ and $N(K - i)$ segments of length j. This is the most equal partitioning of the segments and hence compatible with the maxima in the plane wave CDW. Now we need to prove there is a band gap between the uppermost NK of these orbitals and the other orbitals as the total number of orbitals is NL (and as $t = K/L = NK/NL$). Recall that the molecular orbital energies of a segment of length j are $2\beta \cos(\pi m/(j + 1))$, where m is an integer running from 1 to j. Therefore between each energy level in the segment of length $j + 1$ there is one and only one energy level of the segment of length j. In particular, the NK most antibonding orbitals of the Ni segments of length $j + 1$ and $N(K - i)$ segments of length j correspond to the single most antibonding orbitals of each and every segment. These most antibonding orbitals are seperated in energy from all the other orbitals and hence there is a band gap at hole filling $t = K/L$ as we wished to demonstrate.

The above proof requires that there is a defect near every maximum of the CDW in the ML-unit cell. However the number of defects may be smaller than this number so that there are maxima for which there are no corresponding defects. In such cases it is convenient to introduce a new fictitious defect lattice where a number of defective sites, D, are placed at the maxima for which hitherto there were no corresponding defects. The length of the fictitious unit cell is now $M'L$ where $M' = M + D/L$. The fictitious cell fractional site occupation is N/M' and the fictitious cell fractional hole filling is K/L. The total number of atoms in the fictitious cell is NL ($NL = (N/M')M'L$) and the average length of each segment is L/K. By the arguments outlined in the preceding paragraph, the fictitious cell has a band gap at $t = K/L$.

We now need to demonstrate that in going from the fictitious cell to the true one (which does not contain any of the D fictitious lattice sites) that this band gap at $t = K/L$ is preserved. The difference between the fictitious system and the true system is that in the fictitious system there are segments of either length j or length $j + 1$ which have combined to form segments of roughly doubled size with lengths $2j$, $2j + 1$, or $2j + 2$. In the fictitious system only the top most antibonding orbital of each segment is unfilled. Therefore we need only show that the two highest orbitals of the doubled segment lie above the second highest energy orbital of the halved segments and that the third highest energy orbital of the doubled segment lies beneath the highest energy orbital of the halved segment. This is readily done as we recall that for a segment of length j, its molecular orbital energies are $2\beta \cos(\pi m/(j + 1))$ where m is an integer running from 1 to j. We can in the same way consider tripled and other higher line segment lengths. QED.

The above theorem introduces the quantity $t' = qt$. We may define t' as the effective hole filling. The band gaps of the true hole filling, t, for the defect lattice can be brought into correspondence with the CDW of the effective hole filling, t', of the nondefect lattice. We may similarly define an effective band filling, z', where $z' = 1 - t'$. One may also prove the following converse result.

Theorem: Consider the same system of p_x orbitals as in the preceding case, with fractional site and hole occupancies of respectively q and t. Assume that there is a defect lattice with a band gap at the Fermi energy. The unit cell of this defect lattice is a multiple of the wavelength of the CDW for the nondefect lattice with hole filling $t' \equiv q \cdot t$.

Proof: Assume that the length of the primitive unit cell is M and that N sites in the primitive cell are occupied. Therefore $q = N/M$. By our assumption of a band gap, t must be a rational fraction of N. We therefore can find an integral value K such that $t = K/N$. Therefore $t' = (N/M)(K/N) = K/M$. A CDW for a hole filling of t' has a wavelength of M/K. Recall the unit cell is of length M. QED.

These two results together show that there is a close connection between one-dimensional defect lattices and the CDW of a nondefect lattice with an effective hole-filling t'. In particular the effective hole-filling CDW may be used to produce a defect pattern with a requisite band gap. Furthermore, this CDW based solution is one of the simplest such defect patterns, as all other patterns have unit cells which are integral multiples of this solution.

It is instructive to consider the implications of an effective hole filling versus a true hole filling. There is an alternate way of viewing the effective hole filling. For $t \leq {}^1/_2$, the effective hole filling also corresponds to the case where all vacant sites of the defect lattices are now occupied with fictitious atoms with a complete valence shell of electrons. Thus in the previous example where $q = {}^2/_3$ and $z = {}^2/_3$, we have replaced the missing ${}^1/_3$ lattice sites with atoms for which $z = 1$. The new effective band filling is $z' = ({}^2/_3)({}^2/_3) + ({}^1/_3)1 = {}^7/_9$ and the effective hole filling is ${}^2/_9$. This is the same value as given above in the previous discussion of Figure 3.

Generalizing this result, the effective hole method outlined above corresponds to the following self-consistent strategy to find defect-distortion patterns. We note the band gaps between occupied and unoccupied levels in this paper are generally between σ nonbonding molecular orbitals and σ^* antibonding orbitals. We thus seek to find defect-distortion patterns that open a band gap between such classes of orbitals, i.e., we seek to avoid orbitals that have a combination of σ nonbonding and σ^* antibonding character. Therefore, as done above, we place at each defective site in the lattice an atom, with all its valence orbitals filled, which by a displacive distortion has no bonds with its neighbors. One then calculates at this new electron count the Fermi surface of the corresponding nondistorted, nondefect system. From such a Fermi surface we deduce a k_1 or k_2 vector which nests this Fermi surface to itself. We can in principal find the lowest energy distortion patterns corresponding to these vectors. These distortion patterns in general lead to a band gap between occupied and unoccupied levels. If such a structure has isolated atoms, i.e., atoms which have no bonds associated to them, then the removal of such atoms from the structure maintains the overall band gap. This is so as such isolated atoms are purely nonbonding and therefore a priori their orbitals lie among the occupied bands. If the number of such isolated atoms is equal or greater to the original number of defects in the system, we can in this way generate a defect lattice pattern with a band gap at the required electron count and with the required defect concentration. This method may be seen to be self-consistent as it requires the addition of fictitious atoms,

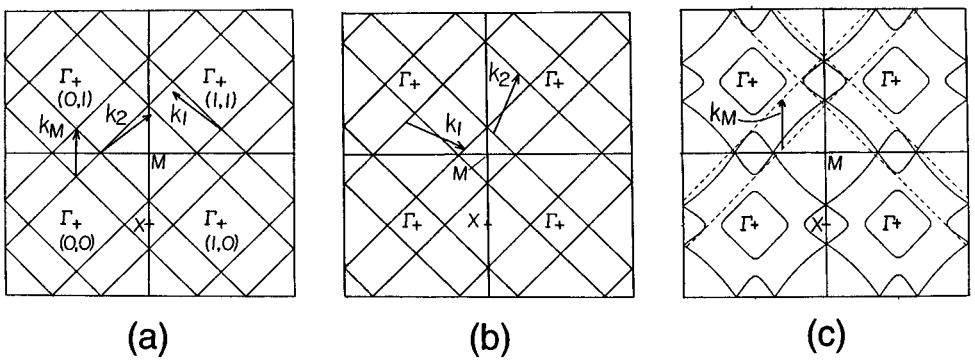

Figure 4. Fermi surface of a σ-model 2-D square lattice for $z = {}^2/_3$ (a) and ${}^4/_5$ (b). The Fermi surface is plotted as a function of reciprocal space. In part a the reciprocal lattice indices are given at Γ. The Fermi surface is along all diagonal lines in the figure. In (c) we show the eH Fermi surface for $K_{0.33}Ba_{0.67}AgTe_2$ where z has the nominal value ${}^2/_3$.

followed by their removal, in order to find a distorted defective lattice which is overall insulating in nature. This is the overall approach taken in this paper. Finally it should be noted that the use of isolated atoms as fictitious units may prove important as the systems studied in this paper are electron rich. Therefore the few unoccupied orbitals in this system have a large number of occupied orbitals with which to interact and the removal of one or two of these does not completely change the overall bonding picture.

Square Lattice d-CDW's

We consider a planar square lattice of main group atoms.[16] In this example we consider only the p orbitals on each atom. We further consider only first neighbor interactions and only σ bonds. We therefore consider only nearest neighbor p_x-p_x, p_y-p_y, and p_x-p_y overlaps, all of which are equal and may be set equal to the same overlap value. In this paper we shall call this approximation the σ model. We consider the two-atom square-lattice unit cell, **2**[17]

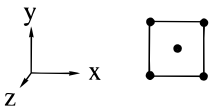

2

In the σ model the p_z orbital is a nonbonding orbital and can be ignored as it is well below the energy of the Fermi level. There are therefore just two active orbitals per atom, and there are a total of four atomic orbitals per unit cell. For every $\vec{k}$-vector there are therefore four crystal orbitals. The energies of these four orbitals are:

$$E_1 = 2\beta \cos[\pi(k_x + k_y)]$$

$$E_2 = 2\beta \cos[\pi(k_y - k_x)]$$

$$E_3 = -E_2$$

$$E_4 = -E_1 \qquad (4)$$

where β is the strength of the σ bond between neighboring p orbitals and where the $\vec{k}$-vector has two indices k_x and k_y as it corresponds to a two-dimensional vector.

We illustrate the shape of the σ-model Fermi surface for $z = {}^2/_3$ and ${}^4/_5$ in Figure 4. The Fermi surface lies on the diagonal lines shown in this figure. The points X and M on this figure correspond respectively to the $\vec{k}$-vectors: $({}^1/_2, 0)$ and $({}^1/_2, {}^1/_2)$. Integral values of the $\vec{k}$-vector correspond to the point Γ. To compare these vectors with those found in diffraction experiments, we note the two-atom square lattice allows diffraction to occur at Γ vectors only, i.e., (h, k), where h and k must be integers and in addition where $h + k$ equals an even number. This latter condition is due to the fact that **2** is a centered cell. In Figure 4a we note the location of four Γ vectors, (0, 0), (1, 0), (0, 1), and (1, 1). We also show in Figure 4c the extended Hückel Fermi surface for $K_{0.33}Ba_{0.67}AgTe_2$ which was calculated using valence s and p orbitals fitted to single ζ-Slater type orbitals, with interactions between atoms up to those 10 Å apart considered. $K_{0.33}Ba_{0.67}AgTe_2$ has tellurium square nets[18] in which the band filling of the p_x and p_y orbitals is $z = {}^2/_3$. Therefore the results in Figure 4c may be directly compared with the idealized Fermi surface shown in Figure 4a. It may be seen that there is similarity between these Fermi surfaces. In the case of the full eH treatment, however, the Fermi surface deviates in a sinusoidal way from the straight line found by the σ model. This has an important consequence. In parts a and c of Figure 4 we indicate the vectors $\vec{k}_M$, which are the maximal nesting vectors. For the simple σ model, as all the Fermi surfaces lie on diagonal line, the vector $\vec{k}_M$ connects every point in the Fermi surface to a corresponding point on the Fermi surface. This vector therefore corresponds to the distortion which allows maximal HOMO-LUMO coupling. By contrast, nesting vectors in the eH model depend explicitly on the observed sinusoidal variations. We therefore take the average of the nesting vectors to find the maximal nesting vector. We find this average nesting vector is (0.35, 0). There is therefore a shift of 0.02 in $\vec{k}_M$-vector length in going from the σ model to the full eH picture. In Table 1 we compare these results with those found experimentally. It can be seen that the average error of this method is 0.03 reciprocal lattice units. The agreement between theory and experiment for both the σ model and the full eH picture are roughly of equal quality.

From the energy expressions given in eqs 4 it is possible within the σ model to derive a simple expression for $\vec{k}_M$ as a function of z or t:

(16) A discussion of the square net is given in: Tremel, W.; Hoffmann, R. *J. Am. Chem. Soc.* **1987**, *109*, 124.

(17) It proves most convenient to consider the two atom square lattice, as in many cases, the actual crystalline superstructure of defective square lattices are not known. Previously published experimental results are presented in terms of the known substructure which is generally found to be the two atom per unit cell square lattice, **2**.

(18) Li, J.; Zhang, X.; Foran, B.; Lee, S.; Guo, H.; Hogan, T.; Kannewurf, C. R.; Kanatzidis, M. G. *J. Am. Chem. Soc.* Submitted for publication.

(19) Bénazeth, S.; Carré, D.; Laruelle, P. *Acta Crystallogr.* **1982**, *B38*, 33.

(20) Marcon, J.; Pascard, R. *C. R. Acad. Sci. Paris* **1968**, *266*, 270.

(21) In the case of $La_{10}Se_{19}$, the chalcogen atoms found between the defective square lattice layers are found to be 3.68 Å distant from the other Se atoms.

Table 1. Theoretically Calculated and Experimentally Estimated Maximum Nesting Vectors, $\vec{k}_M$

	a^*		
compd	σ model	eH	expt[a]
$LaSe_2$	0.50	0.54	0.50
$K_{0.33}Ba_{0.67}AgTe_2$	0.33	0.35	0.33, 0.35
$La_{10}Se_{19}$	0.40, 0.20	0.36	0.40, 0.20
Cs_3Te_{22}	0.45	0.39	0.40, 0.20
$Dy_{65.33}Se_{120}$	0.33	0.29	0.33, 0.28
$RbDy_3Se_8$	0.50	0.49	0.50, 0.25

[a] In the case of the experimental defective lattice systems $\vec{k}_M$ is taken to be $2^{1/2}$ times the projection of the observed nesting vectors along the $a^* + b^*$ direction. For $RbDy_3Se_8$ the observed reciprocal lattice vector is exactly $^1/_2$ of the theoretically predicted cell. Nesting compatible with the Fermi surface is caused by $2\vec{k}$ vs $\vec{k}$ itself.

$$\vec{k}_M = (2z, 0) \qquad 0 \le z \le {}^1/_4$$

$$\vec{k}_M = (1 - 2z, 0) \qquad {}^1/_4 \le z \le {}^1/_2$$

$$\vec{k}_M = (1 - 2t, 0) \qquad {}^1/_2 \le z \le {}^3/_4$$

$$\vec{k}_M = (2t, 0) \qquad {}^3/_4 \le z \le 1 \tag{5}$$

|In particular, the direction of $\vec{k}_M$ is in the pure a^* direction (or by symmetry in the pure b^* direction) and its length is proportional to the number of electrons for $z \le {}^1/_2$, or to the number of holes for $z > {}^1/_2$.

Another case of particular interest is the example where $z = {}^3/_4$, i.e., the p_x and p_y bands are $^3/_4$ filled. For this value $\vec{k}_M = ({}^1/_2, 0)$ and one would expect a real space superstructure two times the size of the original square lattice in the $\vec{a}$ direction. This corresponds with known observed superstructures. In $LaSe_2$ and $CeSe_2$ the square lattice atoms have a net charge of -1 each. If one completely fills both the low-energy 4s and the nearly nonbonding p_z orbital, the p_x and p_y band is $^3/_4$ filled. It is well-established that the square lattice in these systems (which contains no site defects) has a doubled square lattice superstructure.[19,20] Therefore as shown in Table 1 the agreement between the σ model and experiment is in this case exactly correct.

These results for nondefect CDW's may be directly carried over to the case of defect CDW's. To do so we apply the effective band-filling or hole-filling formalism. For example, consider $z = {}^1/_2$ and $q = {}^2/_3$. As $z = {}^1/_2$, we may apply either picture. For the former view we take $z' = zq$ while in the latter one we set $t' = tq$. In either case we find the same $\vec{k}_M$ equal to $({}^1/_3, 0)$.

One can also find direct connections between the band gaps of the defect square lattice and those for the nondefective lattice with effective hole filling, t'.

Theorem: Consider a defective square lattice in the xy plane with lattice sites placed unit distances apart. Let q = fractional site occupation and t = fractional hole filling. Assume that there are a p_x and p_y orbital at every site and that there are only nearest neighbor σ interactions in the system. Assume both that there is a band gap at the Fermi energy and that there is only one defective site per primitive unit cell. Multiples of the defect structure's reciprocal lattice nest the CDW of the nondefect lattice with effective hole filling, t'.

Proof: As the defect structure has a band gap, there must be a defect site in any row or column of the defect structure; an infinite linear chain is gapless. Consider two defects which lie in the same row and for which there is no additional defect between them. Let the distance between these two defect sites be M. Define these points as (0, 0) and (M, 0). Now consider the row directly adjacent to this first row. Choose the defect atom which is closest to the defect site at the origin. This third defect site can be set to lie at (N, 1). We thus construct a unit cell with basis vectors $\vec{a} = (M, 0)$ and $\vec{b} = (N, 1)$. This cell is primitive as by construction no additional defect atom can lie on the borders or interior of the cell. The defect structure therefore consists of linear fragments all of length $M - 1$ all running in the horizontal direction, and the area of the defect primitive cell is M. Furthermore, we may follow the same construction in the columnar direction. As the areas of primitive unit cells are equal we conclude that the defect structure also consists of linear fragments all of length $M - 1$ all running in the vertical direction. We see therefore that as there is a band gap at the Fermi energy, $t = K/(M - 1)$. Furthermore, $q = (M - 1)/M$ and hence $t' = K/M$, where K and M are integers. The corresponding Fermi surface, with respect to a one-atom square lattice, has lines running in the pure vertical or pure horizontal direction with a distance K/M between them.

We further see that $\vec{a}^* = (1/M, -N/M)$ and $\vec{b}^* = (0, 1)$. The Kth multiple of $\vec{a}^*$ nests the t'-effective hole Fermi surface. Choosing the alternate vertical basis set where $\vec{a}' = (0, M)$ and $\vec{b}' = (1, N')$ we find $\vec{a}'^* = (-N'/M, 1/M)$ and $K\vec{a}'^*$ nests the other pair of t'-effective hole Fermi surfaces. QED.

It may be seen that there are clear analogies between the linear chain and the σ-only square lattice. In particular, as long as one of the defects by itself divides the square lattice into finite segments one has produced linear fragments identical in regularity to those found in one dimension. We now consider several specific examples of defect square lattices.

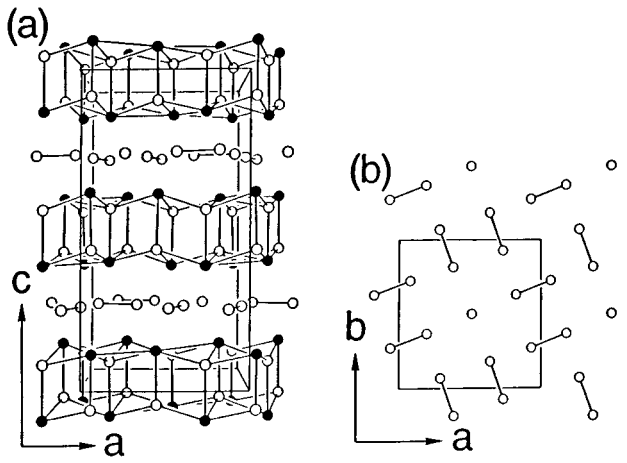

Figure 5. The structure of $La_{10}Se_{19}$. Filled circles are La atoms, open circles Se atoms.

$La_{10}Se_{19}$ and Cs_3Te_{22}

The structures of both $La_{10}Se_{19}$[8] and Cs_3Te_{22}[9] contain defective square lattice sheets of chalcogen atoms. Their structures are illustrated in Figures 5 and 6. In the former system these square lattice sheets are separated by layers of La(III) Se(−II) cubes, while in the latter system the square sheets are separated by Cs(I) and Te_8(0) rings. We assign these oxidation states by assuming that the electropositive alkali metals or rare earth atoms are in their highest oxidative state, and that chalcogen atoms unbonded to other chalcogen atoms[21] have charge −II and that the Te_8 unit which is isostructural with the well-known S_8 molecule is neutral in charge. The structures of the defective square lattices in these systems are shown in Figures 5 and 6. It may be seen that the number of defective sites is 1 and 4 per unit cell for respectively $La_{10}Se_{19}$ and Cs_3Te_{22} and that there are ten potential square lattice sites per unit cell in these systems. The fraction of occupied sites, q, is

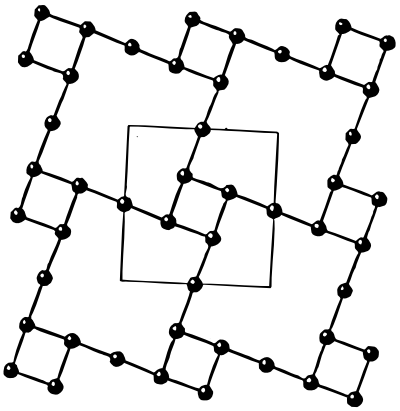

Figure 6. The defective square lattice of Cs_3Te_{22}.

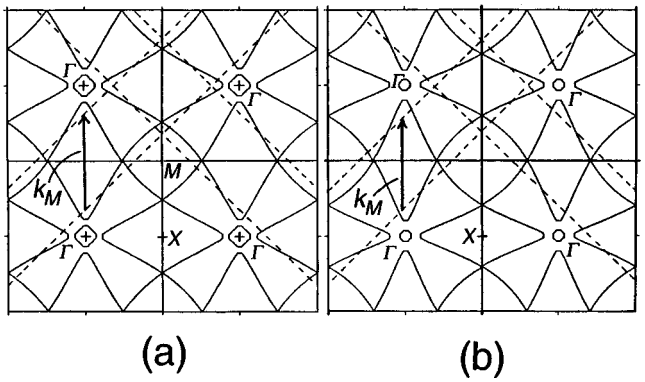

Figure 7. The eH Fermi surface for the defective square lattices of (a) $La_{10}Se_{19}$ and (b) Cs_3Te_{22}. For comparison, the σ-only model Fermi surface is drawn in as a dotted line. It may be seen that the eH surface forms a sinusoidal wave around the average σ-model diagonal lines.

respectively $^9/_{10}$ and $^6/_{10}$. Based on the oxidation assignments given above we may now deduce the average charge on these square lattice sites. In $La_{10}Se_{19}$ we find that of the 19 Se atoms, ten are isolated Se(−II) atoms which are not part of the defective square lattice. Therefore the average charge on each of the atoms in the defective square lattice is $-^{10}/_9$. Similarly in Cs_3Te_{22}, there are two neutral Te_8 rings per unit cell. The average charge on the remaining six Te atoms is $-^1/_2$. To deduce the fractional band occupation, z, of the p_x and p_y band we assume that for every chalcogen atom in the square lattice, four electrons lie in valence s and p_z orbitals. As there are maximally four p_x and p_y e^- per chalcogen atom we find that for $La_{10}Se_{19}$ $z = ^7/_9$ and for Cs_3Te_{22} $z = ^5/_8$. Applying eq 6 we find $t' = (1 - ^7/_9)(^9/_{10}) = ^1/_5 = 0.20$ while for Cs_3Te_{22} $t' = (1 - ^5/_8)(^6/_{10}) = ^9/_{40} = 0.225$. The effective band filling for these two systems is rather similar in value. It can be noted that had there been just one more e^- per Cs_3Te_{22} formula unit the effective band fillings in the two systems would be equal to each other. By contrast, the true fractional band fillings for these two systems differ by the value 0.15. The σ-model Fermi surface for the effective band filling of $t' = 0.20$ was previously given in Figure 4b. In Figure 7 we show the full eH method Fermi surfaces for these two systems. It may be seen that just as in the earlier example for $K_{0.33}Ba_{0.67}AgTe_2$ there is a marked sinusoidal variation in the Fermi surface. Just as in this earlier case we therefore find the average $\vec{k}_M$. These values are given in Table 1. It may be seen that there is reasonable agreement between the eH calculated $\vec{k}_M$ and the simple σ-model result. The possible consequences of this sinusoidal variation are considered in the next section.

The structures of $La_{10}Se_{19}$ and Cs_3Te_{22} differ from those described in the previous section in that there are two independent supercell lattice vectors in these systems. These independent vectors are the two new reciprocal lattice vectors of the supercell. They may be related to the reciprocal lattice vectors of the original 2-atom square cell, **2**, by the formulas:

$$a_n^* = {}^2/_5 a_o^* - {}^1/_5 b_o^*$$

$$b_n^* = {}^1/_5 a_o^* + {}^2/_5 b_o^* \qquad (6)$$

where the subscript n stands for the supercell and o for the original subcell. The existence of two separate vectors can be directly correlated to the two sets of parallel diagonal lines in Figure 4b. In Figure 4b we have labeled two different nesting vectors, $\vec{k}_1$ and $\vec{k}_2$. The vector $\vec{k}_1$ couples the positively sloped diagonal lines to each other while $\vec{k}_2$ couples the negatively sloped diagonal lines to each other. In fact we have chosen $\vec{k}_1$ and $\vec{k}_2$ to be the a_n^* and b_n^* of eq 6. We therefore find that the d-CDW pattern observed experimentally causes nesting of the Fermi surface in agreement with experiment. In the case of $La_{10}Se_{19}$ the agreement between the σ model and the observed unit cell is in exact agreement. The eH method is also in close agreement with the observed unit cell (see Table 1). In Table 1, in order to facilitate comparison of the theoretical and experimental values we have taken the projection of the experimental k vectors along the $\vec{k}_M$ direction. The agreement between theory and experiment for Cs_3Te_{22} however is not as good. We can account for this difference by actually examining the electronic density of states of the defect square-lattice pattern of Cs_3Te_{22}. An extended Hückel calculation on this system shows that at the observed electron count of Cs_3Te_{22}, the defective lattice is metallic. However, had we placed just one additional electron into the Te_6^{3-} square-lattice net, a band gap of 2 eV would appear at the Fermi surface. Thus the equations used for defective CDW's in this paper correctly rationalize what the band filling must be to produce the semiconducting state, as is required by perfect HOMO-LUMO mixing and nesting vector arguments. As HOMO-LUMO mixing generally renders the system more stable, we expect that it should be possible to prepare a perfectly nested defective lattice of the type found for Cs_3Te_{22} for the effective fractional hole band filling of $t' = 0.20$.

It may be seen that while the above results may be used to rationalize the observed superstructure unit cells, they are not precise enough to be of predictive value. For example, though the results are highly restrictive, there are still an infinite number of permissable $\vec{k}$-vectors which couple the Fermi surface to itself. However, the majority of these choices of $\vec{k}$-vectors would lead to direct lattice unit cells of gargantuan proportions. In this, we make a distinction between such hypothetical large unit cells and the incommensurate CDW's found in numerous nondefective systems.[2] In the latter systems, the Fermi surface nesting actually drives the incommensurate CDW. Here the Fermi surface is by itself compatible with a finite sized unit cell. We assume that unless there is a clear driving force, the small direct lattice unit cells will be those most frequently found. In the above cases of Cs_3Te_{22} and $La_{10}Se_{19}$, the observed unit cell is one of the two smallest unit cells compatible with complete nesting of the Fermi surface. The other smallest solution is the one in which $\vec{k}_1 = (^1/_5, 0)$ and $\vec{k}_2 = (0, 1)$. Taking an idea from Pauling's fifth rule[22] for crystal structures, we call such small cells parsimonious.

$Dy_{65.33}Se_{120}$ and $RbDy_3Se_8$

The crystal structures of both $Dy_{65.33}Se_{120}$ and $RbDy_3Se_8$ are only partially known.[10,11] In the case of $Dy_{65.33}Se_{120}$, the

(22) Pauling, L. *The Nature of the Chemical Bond*, 3rd ed.; Cornell University Press: Ithaca, NY, 1960.

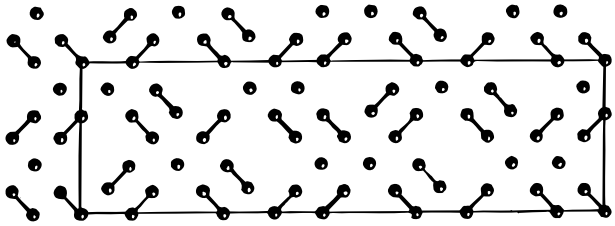

Figure 8. One model of the defective square lattice of $Dy_{65.33}Se_{120}$.

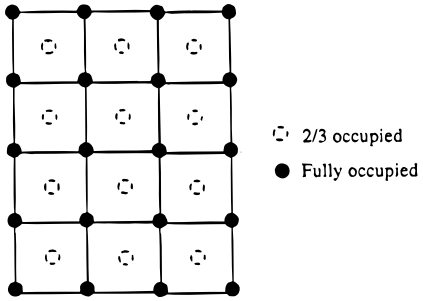

Figure 9. The experimentally determined features of the $RbDy_3Se_8$ defect square-lattice structure. Shown is one superstructure unit cell. Filled circles represent fully occupied sites. Dotted circles represent partially occupied sites, 4 of the 12 such sites are vacant.

structure has been resolved through single-crystal X-ray diffraction to be one of four possible models. The defective square-net of one of these model solutions is shown in Figure 8. In this model, as in the other three, the unit cell contains 66 Se(−II) atoms outside the defective square-lattice sheets and 54 Se atoms in the defective square sheets. Thus there are twelve defective sites on the square lattice. The number of Dy atoms is determined by counting the number of dimers (Se_2^{2-}), trimers (Se_3^{4-}), and other local clusters which exist in the defective square lattice and by assuming charge neutrality. The total fraction of filled Se p_x and p_y orbitals in this system is $z = {}^{43}/_{54}$, while the fraction of occupied sites is ${}^{9}/_{11}$. We therefore find $t' = (1 - {}^{43}/_{54})({}^{9}/_{11}) = {}^{1}/_{6}$.

In a similar manner, we consider the $RbDy_3Se_8$ structure. The unit cell of the defective lattice superstructure is shown in Figure 9. For this system only the substructure and the cell dimensions of the superstructure are known.[10] Of the eight Se atoms per formula unit, three are isolated Se(−II) atoms which lie between the defective square lattices while the remaining five belong to the defective square lattice itself. From these factors we find a fractional band filling of $z = {}^{7}/_{10}$, with $q = {}^{5}/_{6}$ and $t' = (1 - {}^{7}/_{10})({}^{5}/_{6}) = {}^{1}/_{4}$.

We now seek to find for these two systems the superstructure unit cells compatible with these values for t' and q. We shall make the assumption that no square-lattice site in the true superstructure is partially unoccupied. For example, in the $Dy_{65.3}Se_{120}$ structure, ${}^{2}/_{11}$ of the sites are missing, therefore the actual superstructure of the square-lattice cell must be a multiple of 11. We then proceed to find the smallest supercell compatible with the requirement of nesting both sets of parallel diagonal lines of their Fermi surface. The smallest such cell is $k_1 = ({}^{1}/_{3}, 0)$ while $k_2 = (0, {}^{1}/_{11})$. The first vector is the maximal nesting vector for $t' = {}^{1}/_{6}$ while the latter is required by the requirement of complete site occupancy. The final supercell is therefore $3a \times 11b$, a 33-fold increase over the original two-atom unit cell.

It may be seen that the above division of k_1 and k_2 is somewhat arbitrary—with one vector responsible for nesting while the other vector accounts for the full occupancy requirement. It is also possible to produce this same $3a \times 11b$ unit cell in which one chooses two vectors which are each metrically

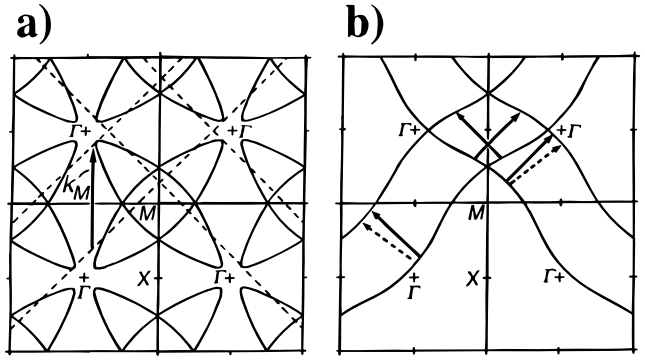

Figure 10. (a) The eH Fermi surface for the defective Se square lattice of $Dy_{65.33}Se_{120}$. Part of the σ-model Fermi surface is drawn as a dotted line for comparison. (b) The sinusoidal curve fitting to the eH Fermi surface—solid arrows show theoretical nesting vectors along $a^* + b^*$, while dashed arrows show the experimentally observed wavevectors.

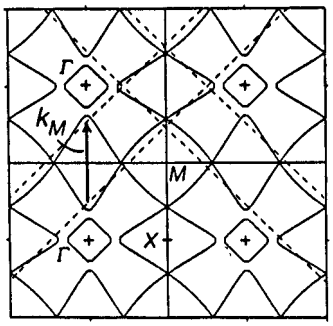

Figure 11. The eH Fermi surface for the defective Se square lattice of $RbDy_3Se_8$. The σ-model Fermi surface is drawn as a dotted line for comparison.

close to the requirement of nesting but have been slightly shifted so as to lead to full site occupancies. One such pair of vectors is $\vec{k}_1 = ({}^{1}/_{3}, {}^{3}/_{11})$ and $\vec{k}_2 = ({}^{1}/_{3}, {}^{-3}/_{11})$. As we show in Figure 4a each of these vectors is close in value to allow nesting. Had the vectors the values of $({}^{1}/_{3}, {}^{1}/_{3})$ and $({}^{1}/_{3}, {}^{-1}/_{3})$, each separately would have led to perfect nesting.

In the case of $RbDy_3Se_8$, the smallest unit cell compatible with the requirements of integral site occupancy and full coupling of the Fermi surface is $\vec{k}_1 = ({}^{1}/_{2}, 0)$ while $\vec{k}_2 = (0, {}^{1}/_{3})$. Weissenberg photographs of this latter system indicate $\vec{k}_1 = ({}^{1}/_{4}, 0)$ and $\vec{k}_2 = (0, {}^{1}/_{3})$. Thus the putative observed structure is twice in size to the cell predicted by the current parsimonious model. It should be noted that a rather complete evaluation of the μ_2-Hückel energy surface of the $RbDy_3Se_8$ structure has shown that the lowest energy Hückel structure has $\vec{k}_1 = ({}^{1}/_{2}, 0)$ and $\vec{k}_2 = (0, {}^{1}/_{3})$. Thus the error in the d-CDW unit cell may not be due to a failure of this principle but may be due to an error in the energy surface of the Hückel method itself. In any case, the observed unit cell in $RbDy_3Se_8$ perfectly nests the calculated Fermi surface, as the new reciprocal lattice vector $2\vec{k}_1$ equals $\vec{k}_M$.

In Figures 10a and 11 we show the Fermi surfaces for the full eH model. It may be seen that in these systems, the sinusoidal variation is particularly great for the $Dy_{65.33}Se_{120}$ system and much less marked for $RbDy_3Se_8$. This sinusoidal variation is due to a combination of π-bonding and second nearest neighbor interactions. In the case of $Dy_{65.33}Se_{120}$ the variation is great enough to imply a breakdown of the pure σ-only model. We show in Figure 10b the sinusoidal Fermi surface in such a way so as to emphasize its nestable nature. The key difficulty in deriving the shape of the Fermi surface exactly is that near Γ there are many states just below the Fermi energy. Mixing of such states will lead to a significant energy

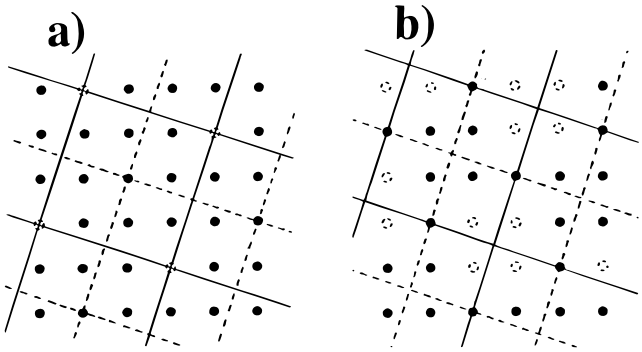

Figure 12. The defect structures of (a) $La_{10}Se_{19}$ and (b) Cs_3Te_{22} viewed as SOW's. Thick lines indicate wave crests, while dotted lines wave troughs. Filled circles represent occupied sites, while dotted circles represent vacant sites.

lowering analogous to a second-order Jahn−Teller effect. The sinusoidal curve shown in Figure 10b is a reasonable low curvature approximation for the region near Γ. The maximal nesting vectors for this surface are also shown. Unlike in the case of the previous σ-only model it may be seen that two vectors are required in order to achieve full nesting. One such vector lies along the $x + y$ direction while the other lies in the $x - y$ direction. It is of interest that these two theoretical vectors are quite close to the actual nesting vectors found in the $Dy_{65.33}Se_{120}$ system (previously shown in Figure 4a). To aid in this comparison we show the experimentally observed superlattice vectors in a dotted line format. As we noted earlier, the experimentally observed superlattice vectors differ from the theoretically calculated ones in that they correspond to a lattice with integral site occupancies on all square-lattice sites. Finally in Table 1 we compare the experimental and theoretical values for the supercell vectors. Variation between the σ model and the eH model are on the order of 0.03 reciprocal lattice units.

Site Occupancy Waves

In our discussion of the one-dimensional d-CDW's, we showed that the lattice defects adopted a wave-like pattern in which the amplitude of the nesting vector could be related to the positions of defects in the lattice. Defects tended to occur at crests of the nesting vector waves and filled occupied sites at troughs; such patterns are site occupancy waves (SOW's). This correspondence could be maintained in two-dimensional systems as well. We therefore consider the defect patterns in the three chalcogenide square-lattice structures with well-characterized defect occupation factors: $La_{10}Se_{19}$, Cs_3Te_{22}, and $Dy_{65.33}Se_{120}$. In the first two systems there are two nesting vectors, $\vec{k}_1$ and $\vec{k}_2$. The resultant overall amplitude, $A(\vec{r})$, has the form:

$$A(\vec{r}) = \cos(2\pi\vec{k}_1\cdot\vec{r} + \theta_1) + \cos(2\pi\vec{k}_2\cdot\vec{r} + \theta_2) \qquad (7)$$

where there are now two arbitrary phase factors, θ_1 and θ_2. The phase difference between θ_1 and θ_2 is variable, and as a consequence the function $A(\vec{r})$ can have considerable variation. The values of θ_1 and θ_2 which accord best with the observed crystal structures are $\theta_1 = \theta_2 = 0$ for $La_{10}Se_{19}$ and $\theta_1 = 0$ and $\theta_2 = \pi$ for Cs_3Te_{22}. In Figure 12 we plot these waves graphically, where we use solid lines to represent wave crests and dotted lines to represent the wave troughs. There is agreement between the assumed positions of these waves and the actual structure. In the case of $La_{10}Se_{19}$, this may be attributed to the assumption that the two waves are in phase at a lattice site position, while in Cs_3Te_{22} the point the waves are assumed in phase is out the center of a square of the overall square lattice. It is clear that the indeterminacy of phase angles θ_1 and θ_2 allows one much too great a latitude in the construction of the theoretical SOW for eq 7 to be of significant practical use.

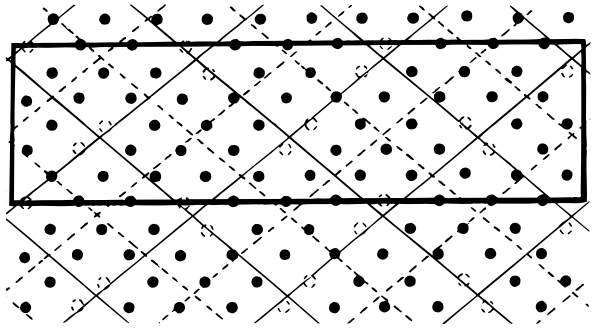

Figure 13. $Dy_{65.33}Se_{120}$ structure viewed as an SOW. See caption of Figure 12 for figure conventions.

We turn to $Dy_{65.33}Se_{120}$. In Figure 13 we show the corresponding wave pattern $\vec{k}_1 = (-1/3, 3/11)$ and $\vec{k}_2 = (1/3, 3/11)$. It may be seen that the unoccupied lattice sites correspond to the intersection of the crests of the two separate SOW's. Just as in the $La_{10}Se_{19}$ system, the intersection of the troughs of the two waves tends to correspond to isolated Se^{2-} atoms. Finally it should be noted that in the original crystallographic work for $Dy_{65.33}Se_{120}$ there were four possible models for the crystal structure. While each crystal model differs in their fine details, all have the same pattern SOW as described above.

Conclusion

In this paper we have shown that by changing the band filling from the actual electron band filling to an effective band-filling we are directly able to apply the Fermi surface of the unperturbed substructure to the defective lattice CDW problem. We have considered four square-lattice systems with such d-CDW's $La_{10}Se_{19}$, $RbDy_3Se_8$, Cs_3Te_{22}, and $Dy_{65.3}Se_{120}$. The methods used are a direct generalization of the pure CDW methods which are used to understand the nondefective lattice of $LaSe_2$ and $K_{0.33}Ba_{0.67}AgTe_2$. We have further applied a variant of the principle of parsimony and have assumed that the smallest unit cell compatible with the requirement of nesting of the Fermi surface and integral occupancy of lattice sites is the most commonly found superstructure. In the case of $La_{10}Se_{19}$ and $Dy_{65.3}Se_{120}$ there is an exact agreement between this unit cell and that which is found experimentally. For Cs_3Te_{22}, the observed structure is in error by one electron to the one predicted by theory. Finally in the case of $RbDy_3Se_8$, the actual superstructure unit cell is double that of the most parsimonious cell. However this larger unit cell does still allow proper nesting of the Fermi surface.

One unfortunate difference between the defect CDW lattice model described in this paper and the ordinary CDW model is that q, the partial site occupancy, is directly a factor in determining both the Fermi surface nesting vector and the size of the direct lattice unit cell, allowing the possibility of a hidden tautology. It should be noted however that the length and direction of the Fermi nesting vector is q multiplied by the fractional band filling. This fractional band filling is quite independent of the number q. In particular we note that this fractional band filling is affected strongly by the fairly random mix of constituent atoms sandwiched between the defective square layers. Therefore the length of $\vec{k}_M$ is not sufficiently determined by q alone. A good example of this was found in

the Cs_3Te_{22} where the calculated Fermi surface and the observed superstructure were in slight disagreement. As noted above, this error is due to the fact that a true gap between occupied and unoccupied bands is found only on the addition of one extra electron per formula unit. The effective band filling method therefore correctly predicts the electron count required for the semiconducting state. We finally note that the effective hole fillings found in the four known systems are $^1/_4$, $^1/_5$, $\sim^1/_5$, and $^1/_6$. These values are much simpler fractions than those of the true band fillings in these same systems and seem almost a logical continuation of the hole fillings of $^1/_2$ and $^1/_3$ found in the nondefective systems $LaSe_2$ and $K_{0.33}Ba_{0.67}AgTe_2$. The simplicity of these numbers does not seem entirely fortuitous.

Acknowledgment. This research was supported by funds from the Petroleum Research Fund and NSF (DMR-9319196). In addition S.L. would like to thank the Alfred P. Sloan Foundation, the J.D. and C.T. MacArthur Foundation, and the Alexander von Humboldt Foundation for fellowships. This work was carried out mainly at the Technical University of Dresden. We therefore particularly thank the gracious host laboratory of Prof. Peter Böttcher. We also thank Dr. Roger Rousseau, Prof. Timothy Hughbanks, and one of the reviewers for their careful reading of our manuscript and for their helpful comments.

JA951965Z